Published in : Metabolomics (2024), vol. 20, n°25
DOI: 10.1007/s11306-024-02094-2
Status : Postprint (Author's version)

FIRST COMPREHENSIVE UNTARGETED METABOLOMICS STUDY OF SURAMIN-TREATED *TRYPANOSOMA BRUCEI*: AN INTEGRATED DATA ANALYSIS WORKFLOW FROM MULTIFACTOR DATA MODELLING TO FUNCTIONAL ANALYSIS

Fanta Fall[1], Lucia Mamede[2], Madeline Vast[3], Pascal De Tullio[4], Marie-Pierre Hayette[5], Paul A. M. Michels[6], Michel Frédérich[2], Bernadette Govaerts[3], Joëlle Quetin-Leclercq[1]

[1]*Pharmacognosy Research Group, Louvain Drug Research Institute (LDRI), UCLouvain, Avenue E. Mounier, B1 72.03, 1200 Brussels, Belgium*
[2]*Laboratory of Pharmacognosy, Center of Interdisciplinary Research on Medicines (CIRM), University of Liège, Liège, Belgium*
[3]*Institute of Statistics, Biostatistics and Actuarial Sciences (ISBA/LIDAM), Université catholique de Louvain (UCLouvain), Louvain-la-Neuve, Belgium*
[4]*Clinical Metabolomics Group (CliMe), Center for Interdisciplinary Research on Medicines (CIRM), University of Liège, Liège, Belgium*
[5]*Department of Clinical Microbiology, Centre Hospitalier Universitaire de Liège, Domaine Universitaire, 4000 Liège, Belgium*
[6]*School of Biological Sciences, The University of Edinburgh, Edinburgh, Scotland*

KEYWORDS: Metabolomics -- Suramin -- *Trypanosoma brucei* -- Mass spectrometry -- Nuclear magnetic resonance

ABSTRACT

Introduction Human African trypanosomiasis, commonly known as sleeping sickness, is a vector-borne parasitic disease prevalent in sub-Saharan Africa and transmitted by the tsetse fly. Suramin, a medication with a long history of clinical use, has demonstrated varied modes of action against *Trypanosoma brucei*. This study employs a comprehensive workflow to investigate the metabolic effects of suramin on *T. brucei*, utilizing a multimodal metabolomics approach.

Objectives The primary aim of this study is to comprehensively analyze the metabolic impact of suramin on *T. brucei* using a combined liquid chromatography-mass spectrometry (LC-MS) and nuclear magnetic resonance spectroscopy (NMR) approach. Statistical analyses, encompassing multivariate analysis and pathway enrichment analysis, are applied to elucidate significant variations and metabolic changes resulting from suramin treatment.

Methods A detailed methodology involving the integration of high-resolution data from LC-MS and NMR techniques is presented. The study conducts a thorough analysis of metabolite profiles in both suramin-treated and control *T. brucei brucei* samples. Statistical techniques, including ANOVA-simultaneous component analysis (ASCA), principal component analysis (PCA), ANOVA 2 analysis,

Published in : Metabolomics (2024), vol. 20, n°25
DOI: 10.1007/s11306-024-02094-2
Status : Postprint (Author's version)

and bootstrap tests, are employed to discern the effects of suramin treatment on the metabolomics outcomes.

Results Our investigation reveals substantial differences in metabolic profiles between the control and suramin-treated groups. ASCA and PCA analysis confirm distinct separation between these groups in both MS-negative and NMR analyses. Furthermore, ANOVA 2 analysis and bootstrap tests confirmed the significance of treatment, time, and interaction effects on the metabolomics outcomes. Functional analysis of the data from LC-MS highlighted the impact of treatment on amino-acid, and amino-sugar and nucleotide-sugar metabolism, while time effects were observed on carbon intermediary metabolism (notably glycolysis and di- and tricarboxylic acids of the succinate production pathway and tricarboxylic acid (TCA) cycle).

Conclusion Through the integration of LC-MS and NMR techniques coupled with advanced statistical analyses, this study identifies distinctive metabolic signatures and pathways associated with suramin treatment in *T. brucei*. These findings contribute to a deeper understanding of the pharmacological impact of suramin and have the potential to inform the development of more efficacious therapeutic strategies against African trypanosomiasis.

Published in : Metabolomics (2024), vol. 20, n°25
DOI: 10.1007/s11306-024-02094-2
Status : Postprint (Author's version)

Introduction

Omics approaches are used to characterize biological systems. Metabolomics analysis is a powerful tool used to investigate the global metabolic changes within an organism or sample (Fall et al., 2022). It involves the measurement of small molecules, known as metabolites, which are involved in various biological processes such as energy transduction, stress responses, and the synthesis of biomolecules. Metabolomics generates large datasets that require rigorous analysis and a set of statistical analyses to determine markers of interest to identify biomarkers for various diseases, evaluate the effectiveness of drugs, study the effects of environmental factors on metabolism and give information on the modes of action or targets of drugs (Fall et al., 2022; Vincent & Barrett, 2015).

Statistical analysis is a vital component of metabolomics research, allowing researchers to extract meaningful insights from the vast amounts of data generated by these experiments. Different statistical techniques (univariate and multivariate analyses) can be used in metabolomics studies, depending on the specific research question being addressed and the type of data being analyzed. ANOVA and ANOVA-simultaneous component analysis (ASCA) are statistical methods that are used in the field of metabolomics to identify and analyze the variations in metabolic profiles when data are issued from a multifactor experimental design (Jansen et al., 2005; Thiel et al., 2017).

Various metabolomics studies have been conducted on the parasitic protist *T. brucei*, which is responsible for sleeping sickness, to better understand its metabolism and the mode of action of compounds interfering with it (Creek et al., 2015; Fall et al., 2022; Nare et al., 2023). This disease is transmitted between humans and domestic animals through the bite of infected tsetse flies, which are endogenous in sub-Saharan Africa. Much research in recent decades has been devoted to the development of new drugs because most available drugs were not efficient and toxic (Fall et al., 2022). One of the drugs to treat sleeping sickness is suramin, a medication that, despite important toxic side effects, is already commercialized for more than a century (Wiedemar et al., 2020). Suramin is classified as an antiparasitic agent and has been reported to have multiple modes of action on trypanosomes and other parasites, but it has also been reported on a variety of other diseases and/ or pathogenic agents (reviewed by Steverding & Troeberg, 2023; Wiedemar et al., 2020)). It works by inhibiting the parasite's metabolism (Fall et al., 2022; Hannaert, 2011; Wiedemar et al., 2020; Willson et al., 1993; Zoltner et al., 2020). A previous study looked also at the metabolomics effects of suramin treatment in *T. brucei* and found that it alters mitochondrial metabolism, increases pyruvate levels and causes a decrease of the total cellular ATP levels in the parasites (Zoltner et al., 2020).

In our work, Hydrophilic Interaction Liquid Chromatography (HILIC) coupled to an orbitrap Q-Exactive mass spectrometer (HILIC-HRMS), and nuclear magnetic resonance (NMR) spectroscopy are used to study the effect of suramin on *T. brucei* through metabolomics assays. The complex datasets originated by both analytical tools were analyzed using robust statistical analyses. The results of the study could provide additional insights into the mechanisms of action of suramin and how it impacts the metabolism of *T. brucei*, which could potentially lead to the development of more effective treatments for African trypanosomiasis.

Published in : Metabolomics (2024), vol. 20, n°25
DOI: 10.1007/s11306-024-02094-2
Status : Postprint (Author's version)

2. Materials and methods

2.1. REAGENTS

LC-MS-grade ammonium formate, formic acid (98%) and fetal bovine serum (FBS) were purchased from Sigma (Bornem, Belgium). HMI-9 medium and phosphate-buffered saline (PBS) were obtained from Thermo Fisher Scientific (Merelbeke, Belgium). Suramin was purchased from Merck Millipore (Germany). LC-MS-grade methanol, acetonitrile, and LC-MS-grade water were obtained from VWR (Louvain, Belgium). Trimethylsilyl-3-propionide acid-d4 (TMSP) and deuterium oxide (D_2O, 99.96% D) were purchased from CortecNet (France). Phosphate buffer powder was provided by Sigma-Aldrich (Karlsruhe, Germany).

2.1.1. PARASITE CULTURE AND SAMPLE PREPARATION

Parasites used were bloodstream forms (BSF) of the subspecies *T. brucei brucei* strain Lister 427 as previously described (Hirumi & Hirumi, 1994). These trypanosomes were cultured in vitro at 37 °C with 5% CO_2 in HMI-9 medium containing 10% (v/v) heat-inactivated fetal bovine serum (FCS), $NaHCO_3$ (36 mM), hypoxanthine (1 mM), sodium pyruvate (1 mM), thymidine (0.16 mM), bathocuprone (0.04 mM), β-mercaptoethanol (20 mM) and L-cysteine (150 mM). Parasites were maintained at densities between 1 X 10^6/mL and 1.5 X 10^6/mL and 100- or 1000-fold dilution was done every 2 or 3 days. The number of live trypanosomes, judged by their motility, were counted by using a Bürker chamber. Cultures were done in triplicate i.e. 24 flasks in total: 12 treated and 12 control (not treated) and 4 time-points. Control parasites and parasites treated with suramin at its EC_{50}[1] of 17.2 nM, as determined with the Alamar blue assay, were incubated and collected at 12, 24, 29 and 48 h after addition of the drug for metabolomics analysis. Parasites were transferred to a microcentrifuge tube and quenched by rapid cooling in a dry ice/ethanol mixture for 20 s. Samples were centrifuged at 1250 rcf for 10 min. A liquid-liquid extraction was performed with 1.5 mL of an acetonitrile/methanol/ water (4:4:2 v/v/v) mixture. Samples were vortexed and incubated for 20 min at 20 °C, then dried under vacuum before reconstitution in 150 µL of ultrapure water. Samples were centrifuged at 4000 rcf for 2 min and the supernatant then transferred into an LC-HRMS vial. In addition to samples, quality controls (QC) were prepared by pooling 10 µL of each sample and injected multiple times. Alternatively, dried samples were dissolved in 400 µL of buffered D_2O at pH 7.4 with TMSP as internal reference and transferred to 3 mm NMR tubes (Bruker) for analysis.

2.1.2. INSTRUMENTATION, DATA ACQUISITION AND DATA PRETREATMENT

2.1.2.1. LC-MS LC-MS was carried out at the MASSMET Platform and Structural Molecular Analysis (ASM) using an ACCELA Autosampler ACCELA 1250 Pump (Thermo Fisher Scientific) and gradient elution with two mobile phase systems consisting of acetonitrile mixed with either solvent A (10 mM

[1] EC_{50} should be read as the half maximal effective concentration that describes the inhibitory effects on the growth of cultured cells, unlike the IC_{50} mentioned later that describes the half maximal inhibitory concentration to describe effects on (purified) proteins.(Borchardt, 2012; Kazakova & Masson, n.d.)

Published in : Metabolomics (2024), vol. 20, n°25
DOI: 10.1007/s11306-024-02094-2
Status : Postprint (Author's version)

ammonium formate, pH 3.8) for positive ionization or solvent B (20 mM ammonium carbonate, pH 9.2) for negative ionization. A ZIC-pHILIC column (4.6 mm X 150 mm, 5 µm) was used for HILIC chromatography. The gradient for positive ionization started at 5% solvent A for 3 min, increased to 95% at 25 min, and stayed at 95% for an additional 5 min before returning to 5% and being equilibrated for 10 min. The gradient for negative ionization started at 8% solvent B for 3 min, increased to 92% at 25 min, and remained at 92% for an additional 5 min before returning to 8% and being equilibrated for 10 min. The flow rate was 0.3 mL/min, the curve gradient parameter was set at 5, the oven temperature was 40 °C, and the total run time was 40 min. An orbitrap Q-Exactive mass spectrometer (Thermo Fisher Scientific) with an electrospray source ionization (ESI) was used for mass spectrometry in positive (ESI +) or negative (ESI-) ionization modes. The auxiliary gas heater temperature was set at 100 °C and the resolution was set at 70,000. Xcalibur software (Thermo Fisher Scientific) was used to control the data acquisition.

The data were preprocessed with Workflow4Metabolomics under Galaxy (Giacomoni et al., 2015). The raw files were first converted to mzXML format using ProteoWizard software (Adusumilli & Mallick, 2017). Centwave was utilized for peak picking detection. Optional data processing steps were implemented to improve the quality of metabolomics analysis, including elimination of background noise, retention of robust features and filtering based on the coefficient of variation between samples and QCs. Samples were normalized to the QCs. Features in the spectra of the biological samples with intensities greater than two-fold compared to the blank samples were retained, while the remaining features were discarded in what represented a second filtering of the features. A Log_{10} transformation was applied to the samples, followed by Pareto normalization to achieve a Gaussian distribution of the data. Subsequently, the data were subjected to a set of univariate and multivariate statistical analyses using the R programming language.

2.1.2.2. NMR NMR spectra were acquired using TopSpin software on a Bruker AVANCE -NEO 500 MHz spectrometer equipped with a cryoprobe. ^{1}HNMR experiments were performed with a NOESY sequence with 128 scans collected over a spectral width of 20 ppm. All spectra were phased and baseline-corrected manually using TopSpin v4. Spectra were stacked and aligned between 80.59.5 ppm using MestReNova v14. Spectra were divided into buckets of 0.04 ppm, integrated to the sum of intensities and normalized to the number of parasites per sample. Statistical analysis was performed with R software under R-Studio. Lastly, the spectra were annotated using Chenomx NMR Suite 9.0 database and the Human Metabolome Database (HMDB) (Wishart et al., 2007).

2.2. STATISTICAL ANALYSIS

The statistical analyses, reporting and result visualization were performed under R-studio and the functional analysis was done with MetaboAnalyst (Pang et al., 2021).

The main statistical analysis used in this work, "twoway analysis of variance (ANOVA 2)" modeling, was applied to each feature to identify the list of significant features involved in the differentiation of parasite groups with respect to treatment, time and treatment*time interaction.

Published in : Metabolomics (2024), vol. 20, n°25
DOI: 10.1007/s11306-024-02094-2
Status : Postprint (Author's version)

To reduce type 1 error (false positives) and increase the reliability of statistical inference, the FDR correction method proposed by Benjamini-Hochberg (BH) was used (Benjamini & Hochberg, 1995). The Benjamini-Hochberg procedure is a widely used FDR correction method that adjusts the p-value threshold based on the number of tests conducted and the expected proportion of false positives. The mathematical expression used to compute the adjusted p-value is as follows:

$$p - val_I^{BH} = min\left(\frac{p - val_i \times m}{i}, 1\right)$$

where *m* is the total number of features and *i* the index of the ordered p-values before correction. The number of significant tests for each factor in the ANOVA model was compared both before and after False Discovery Rate (FDR) correction.

Different techniques were used to study globally metabolomics data matrices issued from LC-MS and NMR analysis. These methods include first PCA as dimension reduction to visualize the data and identify potential outliers. Multivariate analysis techniques ASCA + and APCA + were also applied to highlight the effects of various factors in the experimental design on each response matrix (Thiel et al., 2017). These methods use the general linear model to calculate matrices effect M_f and bootstrap to test their global significance. For the current design, the response matrix is decomposed as follows:

$$Y = \hat{\mathrm{M}}_0 + \hat{\mathrm{M}}_{Treat} + \hat{\mathrm{M}}_{Time} + \hat{\mathrm{M}}_{Treat*Time} + E$$

and PCA applied to visualize each matrix effect and provide rich complementary information to ANOVA 2 results. ASCA + and APCA + address the issue of bias encountered in parameter estimation when applying ASCA and APCA to a dataset derived from an unbalanced experimental design. The R package limpca (for Linear Models with principal component effect analysis) was used for all these multivariate analyses (Thiel et al., 2023).

2.2.1. FUNCTIONAL ANALYSIS

For LC-MS data, the functional analysis was performed using the second version of the *mummichog* algorithm proposed by Li et al. and implemented in MetaboAnalyst v. 5.0 (Li et al., 2013; Pang et al., 2021). This algorithm combines the steps of metabolite identification and pathway enrichment analysis based on the assumption that false matches are distributed randomly while true matches should show local enrichment. The inputs for the algorithm were the complete list of features and a sub-list containing the significant features. The functional analysis was performed separately for each ANOVA 2 model effect and features with an adjusted *p*-value < 0.05 were considered significant.

The first step of the algorithm is the identification of potential metabolites by comparing the *m/z* of the features to the mass of the compounds belonging to the metabolism of *T. brucei* found in the KEGG pathway library. These metabolites are then mapped to their respective pathway and a Fisher's exact test (FET) is performed for each pathway. In addition to the FET *p*-value, the *mummichog* algorithm computes a permutation *p*-value and an EASE score. The latter is obtained by removing a significant compound from the pathway and then performing a FET on the resulting table.

Published in : Metabolomics (2024), vol. 20, n°25
DOI: 10.1007/s11306-024-02094-2
Status : Postprint (Author's version)

The second version of the *mummichog* algorithm uses the retention time of the features to compute empirical compounds. These empirical compounds are intermediates between the *m/z* features and the compounds. The algorithm separates one compound into two empirical compounds if the difference of retention time between the corresponding features is larger than expected. Isomers are also regrouped in one empirical compound. The algorithm then performed the pathway enrichment analysis based on these empirical compounds (Pang et al., 2020).

MetaboAnalyst produces two output tables. The first contains the potential matches, the corresponding features and empirical compounds. The second contains the results of the pathway enrichment analysis: the pathways, the number of hits, the *p*-values and the list of significant empirical compounds from the data included in the pathways.

For biological interpretation, the compounds in the significant pathways are needed. Indeed, based on the assumption of the algorithm, these compounds are more likely to be correctly matched to the features. In our work, the pathways with an EASE score < 0.05 are considered as significant. However, a list of the potential compounds in these pathways is not directly available in the MetaboAnalyst outputs. It is retrieved by comparing the list of potential matches from MetaboAnalyst and the list of compounds belonging to each pathway from the KEGG pathway library. This comparison is performed in R and the KEGG pathway library is accessed using the package KEGGREST.

In addition to retrieving the compounds in significant pathways, the corresponding features are also retrieved. This allows to visualize the evolution of their intensities over time by treatment.

3. Results and discussion

3.1. DESCRIPTIVE UNTARGETED METABOLOMICS ANALYSIS

BSF *T. brucei* 427 cells were cultured in vitro in the absence of suramin, or in the presence of 17.2 nM of this trypanocidal drug. This concentration corresponds with the EC_{50} value as determined in a 72 h Alamar Blue assay. As shown in Supplementary Fig. 1, no effect on cell density is yet observed during the first 12 h, but upon further culturing until 48 h, growth of the trypanosomes is inhibited by about 30.3% compared to the control. Samples were taken after 12, 24, 29 and 48 h of incubation and processed for metabolomics analysis as described in Materials and Methods. The samples were analyzed by liquid chromatography (HILIC) coupled with both positive and negative ionization MS and NMR techniques. Following mass spectrometry analysis, 5357 and 2607 metabolites were detected respectively in positive and negative ionization modes. After applying filtering steps to improve sample quality, a set of features were removed. 1546 and 1654 features were kept and subjected to multivariate and univariate statistical tests.

NMR proton spectra were obtained and transformed as described in the Materials and Methods section and binned in equal intervals which amounted to 180 bins per sample. This bin table was used directly for multivariate and univariate statistical analyses. In parallel, the spectra were

Published in : Metabolomics (2024), vol. 20, n°25
DOI: 10.1007/s11306-024-02094-2
Status : Postprint (Author's version)

annotated through the Chenomx NMR Suite 9.0 database and the HMDB which identified up to 42 metabolites.

3.2. STATISTICAL ANALYSIS OF THE METABOLOMICS RESULTS

3.2.1. PRINCIPAL COMPONENT ANALYSIS (PCA): SCORE PLOTS

Principal component analysis (PCA) allows for a first exploratory data analysis. The score plots in Fig. 1 A and C show that, for the MS-negative and NMR data, a separation is observed between the groups treated with suramin and the control groups. The cumulative contribution of the first two principal components (PC1 + PC2) accounts for a significant proportion of the total variance observed in these two analytical conditions (52.3%, 38.05% and 67.4%, respectively). The treatment effect is less visible in the PCA graph of the MS-positive as shown in Fig. 1 B, and the % of variance explained by the two first of principal components is only 35.0%. In all three graphs, the effect of kinetics is also clearly visible on the first component. These findings suggest that both treatment and time affect the resulting data. Finally, note that one strong outlier has been removed from the NMR data after a preliminary PCA analysis, which then originated the score plot of Fig. 1C.

3.2.2. ASCA MODELING RESULTS

Table 1 displays the global percentage of variance explained by each model effect factor calculated by the ASCA ANOVA decomposition, as well as the corresponding bootstrap *p*-values. The table includes four sources of variation: treatment, time, the interaction between treatment and time, and residuals. The residual score plot represents the noise in the data when all model effects have been removed.

These results confirm the PCA observations: treatment and time have a significant effect on the metabolomics spectral profiles for MS-positive, MS-negative and NMR results and the interaction is significant for MS-negative and NMR spectra only. For MS-positive results, the three effects are less significant because the percentage of variance attributed to noise (residuals) is higher (51.4%). For MS-negative and NMR results, most of the variance is explained by the two main effects (treatment and time) as observed in PCA (49.4% and 55%, respectively). Interaction effects, although of lesser importance in comparison to other results, are of particular interest in this study since they indicate that the evolution over time of certain metabolites differs between treated and control samples.

Figure 2 complements Table 1 with the APCA score plots resulting from the PCA decomposition of matrices effect. In APCA, each matrix effect is initially enhanced by the residuals, enabling a visual comparison between the factor effects and the data's noise. Each score plot must then be seen as a representation of the data with respect to one model effect after having removed the effects of others.

The treatment score plots allow to observe a clear separation of treated and control samples for MS-positive and NMR data on the first PC axis and the time score plots show, from left to right a quite clear evolution of the samples over time. The corresponding PCA loading (provided by Fig. 1) allowed to identify features linked to each effect. Finally, PCA on residuals are mostly useful to highlight new

Published in : Metabolomics (2024), vol. 20, n°25
DOI: 10.1007/s11306-024-02094-2
Status : Postprint (Author's version)

outliers after the ANOVA decomposition and can be found in Supplementary Fig. 2. No important outliers appear in these graphs.

3.2.3. UNIVARIATE ANOVA 2 STATISTICAL MODELING: NUMBER OF SIGNIFICANT FEATURES

ASCA global spectral analysis was then complemented by an individual ANOVA 2 modeling of each feature (bins in NMR and *m/z*—peaks in MS) in order to identify, *in fine*, which metabolites are significantly affected by treatment, time or their interaction. Table 2 presents the number and

percentage of significant features as a function of the effect involved in the ANOVA 2 model before and after multiplicity correction. The reduction in the number of features observed after each BH-FDR correction for each effect allows to remove potentially false positives and control the global error rates. For example, for the factor treatment, there is a reduction from 44 to 37% for MS-positive, from 28 to 14% for MS-negative, and from 53 to 45% for NMR. These lists of significant features have been further compared to ASCA important ones and used for metabolites and pathways identification.

3.2.4. VISUAL IDENTIFICATION OF FEATURES OF INTEREST ON THE BASIS OF ASCA AND ANOVA 2 RESULTS

When the number of features is high in a multivariate analysis, it is quite difficult to evaluate graphically their importance. In this paper, the *p*-values of the ANOVA 2 modeling were mainly used to identify important metabolites and linked pathways. Nevertheless, features (MS-peaks or bins) of importance based on ANOVA 2 *p*-values and ASCA loadings can be represented graphically among each other by scatter plots to check the relation between both and detect the most important ones located at the top-right of the graphic. Such graphics are provided for information in Supplementary Fig. 3 for the NMR analysis. They can be interpreted similarly to volcano plots in transcriptomics.

3.2.5. IDENTIFICATION AND FUNCTIONAL ANALYSIS OF METABOLITES

Supplementary Fig. 4A and B show the evolution of the number of *m/z* features at the steps of the ANOVA, identification of potential matches and in significant pathways for the MS data in negative mode and positive mode, respectively. For the MS data in positive mode, there are not enough significant peaks to perform the functional analysis for the interaction effect. For the treatment and time effect, no significant pathways have been identified by the *mummichog* algorithm. Potential compounds for the significant features from MS data in positive mode have been computed based on the mass-to-charge ratio and are included in Table 3.

Table 4 shows metabolic processes significantly impacted by each effect and the potentially significant matches included in these processes for the MS data in negative mode. Five processes are significantly impacted by the effects. One or more processes involving amino acids, most likely protein synthesis as will be discussed later in this paper (Results and Discussion Sect. 4), and nucleotide-sugar metabolism, are significantly impacted by the treatment. Metabolites that have been significantly impacted by the time are those of the metabolism of di- and tricarboxylates (the former involved in succinate production and both in the TCA cycle) and possibly processes of amino-

Published in : Metabolomics (2024), vol. 20, n°25
DOI: 10.1007/s11306-024-02094-2
Status : Postprint (Author's version)

acid metabolism linked to the latter. Finally, two pathways involved in sugar metabolism have been impacted by the interaction of the two factors: glycolysis and galactose metabolism.

ANOVA of the NMR data indicated 81 bins out of 180 bins as significative between suramin and control, of which 3 were significative for the interaction as well. Out of these, 75 bins were annotated mainly with the Chenomx NMR Suite 9.0 database, which represents a significant majority of the spectral peaks (92.6%). However, it is worth mentioning that bins (Wishart, 2010) are a matrix representation where each characterizes a set width interval of the original spectrum, in ppm in this case. Because of the physico-chemical properties of metabolites, they will appear in one or multiple clusters in which the peaks can have variating multiplicities in a wide range of ppm (NMR-Based Metabolomics, 2018). As such, similar molecular groups or positions will elicit peaks in the same spectral area, leading to overlapping signals within one bin. This disadvantage of the small chemical shift window of 1HNMR makes annotation and interpretation of significant bins a bit more challenging, but still relevant and interesting in the context of cross-analysis and biological interpretation.

A panel of metabolites has been identified to delineate distinct effects using NMR and LC-MS analyses. Some metabolites have been detected utilizing both analytical methods, while others are selectively discernible through either of them. A comprehensive summary of the detected metabolites, accompanied by their respective degrees of statistical significance, is presented in Table 5.

4. Biological interpretation

Functional analysis of suramin-treated versus control BSF *T. brucei* using LC-MS data and NMR annotation revealed that the main metabolites modulated by treatment, time, or interaction effects participate in various processes of the cells. Metabolites that are significantly changed are listed in Table 4 and, in a time-dependent manner of their changes shown in the heatmaps in Fig. 3 and Fig. 4. The observation of multiple changes is in agreement with the notion that this drug may have several targets in trypanosomes (Hannaert, 2011; Wiedemar et al., 2020; Willson et al., 1993; Zoltner et al., 2020). Some of the metabolic changes observed may be primary effects, directly attributable to the inhibition of a specific target, whereas others may be secondary, resulting from effects such as a cellular energy collapse, changes in protein expression and/or accumulation of metabolites in ways that are affecting other processes. Here we will discuss several metabolic changes observed in our study.

Most strikingly, in both the LC-MS and NMR analysis, intensities of many amino acids were found to be higher in parasites treated with suramin when compared to the control (Fig. 3, 4 and 5). However, the time dependency differed between the two studies.

For LC-MS, an increase in some metabolite intensities was observed at 12 h in the samples treated with suramin compared to the control samples at 12 h as seen in Fig. 3. In the case of NMR, this increase is only statistically significant at 29 h compared to the control samples at 29 h. This may be

Published in : Metabolomics (2024), vol. 20, n°25
DOI: 10.1007/s11306-024-02094-2
Status : Postprint (Author's version)

explained by the different sensitivities of the two methods, as well as the differences in data normalization and statistical analyses. When focusing on the treated samples and the time effect, a gradual decrease in metabolite intensities is observed over time. The pathway analysis by MetaboAnalyst highlighted amino-acyl tRNA synthetase, the enzyme that recognizes an amino acid and its cognate tRNA, as a likely suramin target responsible for the higher intensities. However, trypanosomatids, like cells in general, possess distinct synthetase enzymes for different amino acids (Nasim & Qureshi, 2023). Indeed, 26 aminoacyl tRNA synthetases have been recognized and, at least forral of them, decreased activity associated with inhibition of parasite growth. These highly diverse enzymes have been the focus of studies to develop inhibitors that would target these trypanosomal enzymes (reviewed recently by Kushwaha & Capalash, 2022; Nasim & Qureshi, 2023)) Based on this information, we consider it more likely that the accumulation of many amino acids as observed upon suramin treatment in our study is caused by inhibition of a common downstream step in protein synthesis.

The HMI-9 medium in which the trypanosomes were cultured is rich in amino acids, rendering it likely that they are taken up by active transporters rather than being synthesized de novo (Marchese et al., 2018). The later decline in intensities as observed by LC-MS may be due to a different, more delayed aspect of the suramin treatment, such as an ATP depletion (discussed below) inhibiting the active transport processes and/or the formation of peptide bonds. In this respect, it is noteworthy to mention that recently published data showed that protein synthesis accounts by far for most of the ATP consumption in bloodstream-form *T. brucei* (Nascimento et al., 2023).

Changes in protein levels have been observed in the proteomic analysis of suramin-treated BSF trypanosomes in the study by Zoltner et al. (Zoltner et al., 2020). However, these changes observed after 48-h of treatment—also with the drug present at EC_{50} (in that study, 35 nM)—were not attributed to a direct effect of the drug on translation, but to a reprogramming of the proteome resembling the changes that occur when BSF trypanosomes differentiate to insect-stage specific procyclic forms. This suramin-induced proteome change was possibly due to an alteration of the cell's energy state.

Major suramin-induced changes were observed for various glycolytic intermediates. BSF *T. brucei* depends for its ATP production entirely on glucose catabolism (Fig. 6) of which the end-products are excreted. The predominant product is pyruvate, formed via the glycolytic pathway. Minor glucose-derived end-products are: (i) alanine converted from pyruvate by the addition of an amino group transferred from a different amino acid, (ii) succinate, produced from the glycolytic intermediate phosphoenolpyruvate (PEP) via the dicarboxylic acids oxaloacetate, malate and fumarate as intermediates, and (iii) acetate, formed from pyruvate in the mitochondrion, where acetate can also be produced by oxidation of threonine (Mazet et al., 2013). Unique for trypanosomes and related protists is the compartmentalization of the first 7 of the 10 enzymes of the glycolytic pathway in peroxisome-related organelles called glycosomes, whereas the last three, including pyruvate kinase responsible for the net ATP synthesis, are present in the cytosol (Fig. 6) (Michels et al., 2021; Opperdoes & Borst, 1977). The enzymes of the succinate-producing pathway are also sequestered within the glycosomes. In our LC-MS study, intracellular intensities of glucose and several glycolytic intermediates were found to be higher in suramin-treated trypanosomes within 12 h, followed by a

Published in : Metabolomics (2024), vol. 20, n°25
DOI: 10.1007/s11306-024-02094-2
Status : Postprint (Author's version)

gradual decline (Fig. 5). The intermediates that changed in this manner are the products of the first three enzymes of the pathway present in glycosomes: glucose 6-phosphate (G6P), fructose 6-phosphate (F6P) and fructose 1,6-bisphosphate (FBP) as well as those of the last three cytosolic enzymes: 2-phosphoglycerate (2PG), PEP and pyruvate. Zoltner et al. (2020) also reported higher intensities of F6P and FBP, although only after 21 h (Zoltner et al., 2020). The most significant difference they observed concerned pyruvate; only slightly higher after 12 h, but a nearly fivefold higher intensity after 21 h. In contrast to our study, they reported a 50% drop of PEP at 21 h. Intracellular intensities related to succinate and acetate, also in part end-products of glucose catabolism, were higher too within 12 h.

Intriguingly, Willson et al. (Willson et al., 1993) reported previously that suramin inhibits all *T. brucei* glycolytic enzymes purified from glycosomes with IC_{50} values varying from 3 to 100 µM. However, these values are over 100-fold the concentration required to kill trypanosomes, EC_{50} = 17.2 nM in our study. Previous studies demonstrated that suramin enters trypanosomes predominantly by endocytosis after binding to the surface protein ISG75 and is then, via the lysosome, delivered to the cytosol (Alsford et al., 2012; Zoltner et al., 2015). This process leads to accumulation of the drug: ninefold, up to an intracellular concentration of 1.8 pM under the experimental conditions used by Zoltner et al., 2020. However, it is possible that the highly negatively-charged suramin concentrates specifically within glycosomes, by tightly binding to the glycosomal glycolytic enzymes with their high pK values (8.8-10.2) (Misset et al., 1986). Given that the ~ 60 glycosomes in BSF trypanosomes comprise together about 5% of the cellular volume, an additional ~ 20-fold concentration of the drug may then be possible. Assuming also a ninefold accumulation within the trypanosomes in our experiments performed at an extracellular suramin concentration of 17.2 nM, an intraglycosomal concentration of 3 pM would be achievable, corresponding to, or not far below the IC_{50} values of some glycosomal enzymes (Willson et al., 1993). Suramin (1297 Da) would be too large for entering glycosomes by free diffusion through the pores in their membrane (allowing passage of molecules up to 400-500 Da (Michels & Gualdrón-López, 2022)), but it is conceivable that it could enter while bound to the newly synthesized proteins that are post-translationally imported. With a doubling time of approximately 6 h of BSF *T. brucei* in HMI-9 medium, implying ~ 75% new glycosomal protein content being formed after 12 h, and > 90% after 24 h, such a scenario would have provided sufficient time to accumulate suramin at low micromolar concentration within the organelles during the experimental conditions used. This is consistent with the metabolic changes that occur after 12 h of incubation between treated and control samples in our study, which evidences, along with the loss of relative viability as shown in Supplementary Fig. 1, that these are correlated to suramin's mode of action and not to a mode of death.

Besides inhibiting some individual glycosomal enzymes, it is also conceivable that the tight binding of suramin to glycosomal proteins may prevent and/or disrupt the interaction between the glycosomal enzymes, known to exists as a multienzyme complex (Misset et al., 1986), as also proposed by Zoltner et al. (Zoltner et al., 2020). Such disassembly of the complex will likely affect the glycolytic flux, the concentrations of glycolytic intermediates and the production of ATP. It may also be responsible for the minor changes in glycosomal morphology reported by these authors, although these may also be due to the drop in cellular ATP, since glycosomal biogenesis involves the

Published in : Metabolomics (2024), vol. 20, n°25
DOI: 10.1007/s11306-024-02094-2
Status : Postprint (Author's version)

activity of cytosolic AAA-ATPases (PEX1 and PEX6 (Michels & Gualdrón-López, 2022)). It should be noted that ATP could not be detected in the datasets of our metabolomics studies.

The pyruvate accumulation detected both by Zoltner et al. and by us is surprising, because previous studies did not show any control of pyruvate efflux on the glycolytic flux (Bakker et al., 1999) and pyruvate is expected to exit the cell electroneutrally in symport with a proton by a facilitated diffusion carrier, following the transmembrane gradient (Wiemer et al., 1995). The exit would thus not be limited when the external pyruvate concentration is below the intracellular one. To assess if suramin inhibits the transport, Zoltner et al. overexpressed the transporter, but this did not protect trypanosomes from suramin toxicity. Thus, one may wonder if the overexpressed transporter molecules were functional. The alternative explanation is an increased pyruvate production from PEP, either via the cytosolic pyruvate kinase or the glycosomal pyruvate, phosphate dikinase (PPDK) (Fig. 6). Zoltner et al. favored PPDK, because a threefold higher expression of this enzyme (after 2 days), typical for the procyclic form, was observed. However, increased activity of pyruvate kinase is equally feasible, because of the significantly higher level of its allosteric activator FBP (Ka = 0.26 mM (Morgan et al., 2014)). Nonetheless, the observation that the intensities of PEP and 2PG, the metabolites directly upstream of pyruvate, are higher suggests that pyruvate accumulation is due to a downstream process such as partial inhibition of its efflux rather than resulting from an increased activity of pyruvate kinase or PPDK. Moreover, pyruvate kinase is highly expressed in BSF *T. brucei*, in substantial overcapacity, whereas PPDK is almost undetectable (Bakker et al., 1999; Bringaud et al., 1998). It is thus questionable that a mere threefold increase in PPDK expression would lead to a significant change in pyruvate.

Other metabolites of which the intensities were impacted are dicarboxylic acids (oxaloacetate, malate, succinate) which are intermediates of both the TCA cycle and the glycosomal succinate production pathway. In addition, several amino acids with higher intensities are directly connected to intermediates of the TCA cycle (e.g., proline, glutamate; Fig. 6). Since both in our analysis and that by Zoltner et al. (2020) these changes were observed after 12 h, they may be considered as primary effects of the suramin treatment, although the increased expression of enzymes of the mitochondrial TCA cycle and glycosomal succinate-producing shunt were only apparent at later stages.

Intermediates of nucleotide-sugar biosynthesis, aminosugar biosynthesis and galactose metabolism were also affected by suramin treatment. Nucleotide-sugars and amino-sugars are important for the synthesis of glycoproteins and glycosylphosphatidylinositol by which surface (glyco-)proteins can be anchored to the lipid bilayer of the plasma membrane. The primary building blocks for these biosynthetic processes are the sugar-phosphate intermediates (G6P, F6P) of the glycolytic pathway. It is therefore not surprising that the synthesis of nucleotide- and aminosugars is affected when the availability of the building blocks change, although a primary effect by suramin on these biosynthetic processes can currently not be excluded. Similarly, for galactose metabolism that is also intricately linked with the sugar-phosphate intermediates of glycolysis. Although G6P serves also as the substrate for the pentose-phosphate pathway, our analysis did not reveal significant changes in the intensity of any of its intermediate metabolites.

Published in : Metabolomics (2024), vol. 20, n°25
DOI: 10.1007/s11306-024-02094-2
Status : Postprint (Author's version)

5. Conclusion

In metabolomics, having a comprehensive analysis workflow is crucial to obtain robust and reliable biological results. The combination of univariate and multivariate statistical analyses, along with development of statistical tools and packages, allows for continuous improvement in metabolomics analyses. In this workflow, corrections were applied, leading to the elimination of a significant number of false positives and resulting in better identification of statistically significant metabolites. The use of ASCA tools in this study allowed us to identify significant effects and their percentage contributions to the observed separations in the PCA plots, for example.

In LC-MS, functional analysis tools facilitated improved identification of the metabolic pathways modulated by the different tested effects. However, our work also highlights the limitations in the identification of molecules and metabolic pathways involved in various biological processes. Despite the significant progress brought by functional analysis tools, there is still much work to be done to enhance metabolomics identification analyses.

NMR is a frequently-used tool in the field of metabolomics and emerges in this work as an important, simple and quick tool to valorize and confirm the data obtained by LC-MS analysis. Although both NMR and LC-MS involve expensive hardware to acquire and maintain, the complimentary of the techniques as demonstrated in this work displays the interest in this association and the fruitful outcome of collaborations between LC-MS and NMR-based research facilities. Our study demonstrated that suramin affects multiple processes in *T. brucei*, most notably pathways involved in the parasite's energy metabolism and processes involving many amino acids, possible protein synthesis. Further studies incorporating fluxomics would provide a better understanding of the catabolic and anabolic mechanisms by which the identified metabolites are changed by the drug.

Published in : Metabolomics (2024), vol. 20, n°25
DOI: 10.1007/s11306-024-02094-2
Status : Postprint (Author's version)

Figure 1.

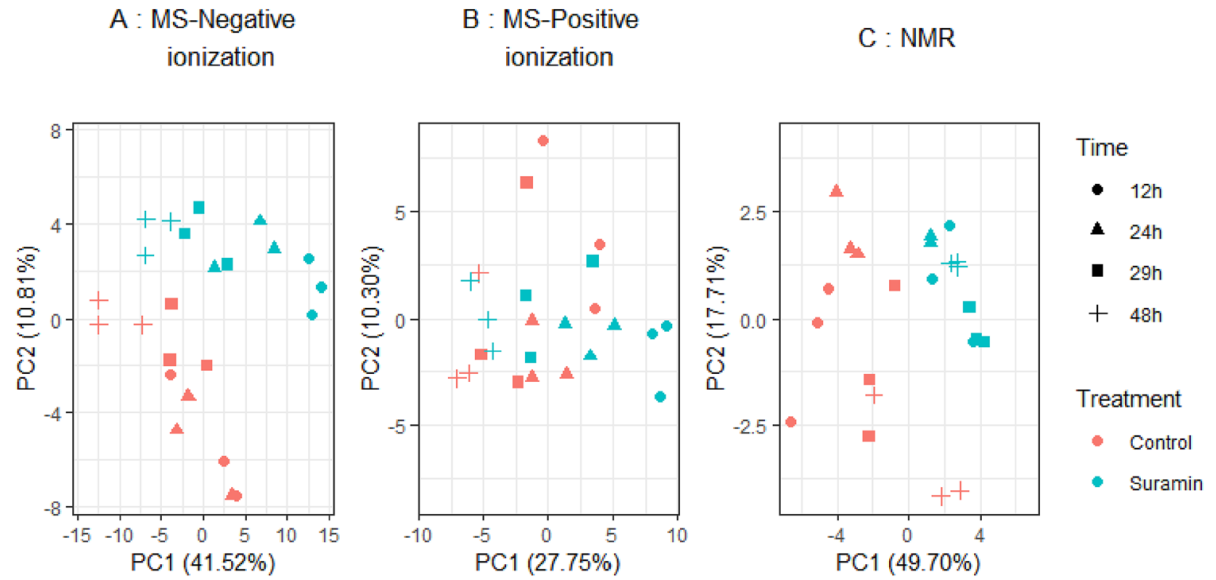

Exploring treatment and time effects on suramin-treated versus control *T. brucei* samples: a comparative principal component analysis study at 12, 24, 29, and 48 h. **A** MS-negative ionization, **B** MS-positive ionization and **C** NMR analysis.

Figure 2.

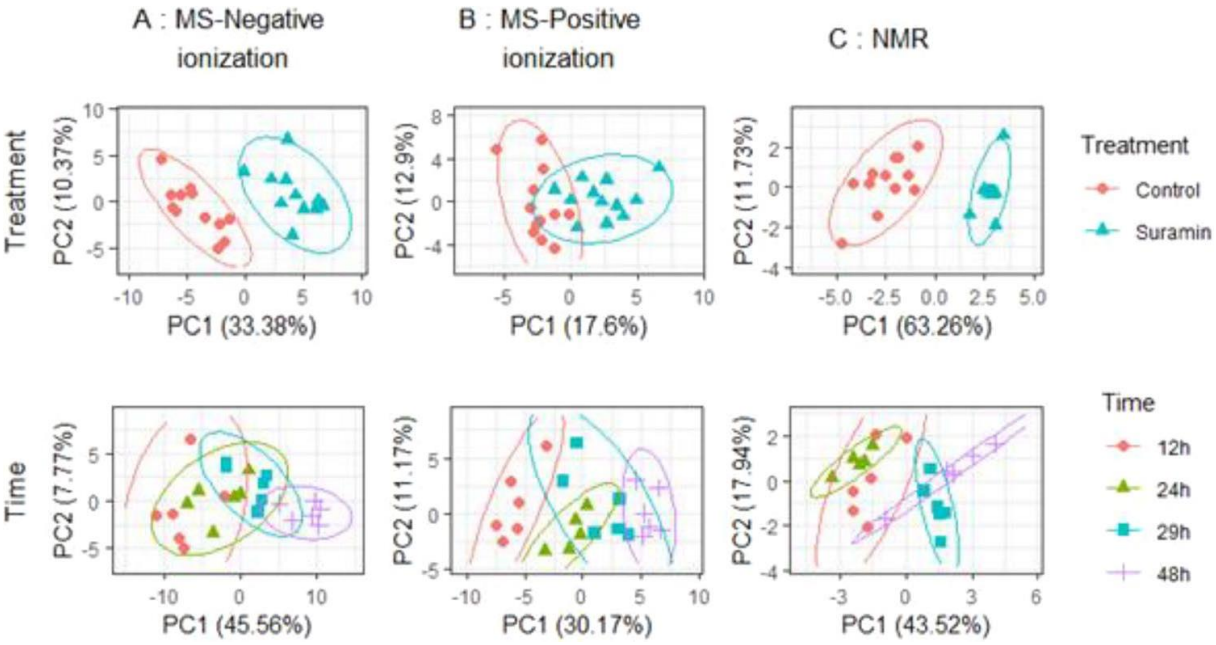

APCA score plots resulting of the PCA on the augmented effect matrices for the three analytical methods. **A** MS-negative ionization, **B** MSpositive ionization and C: NMR analysis.

Published in : Metabolomics (2024), vol. 20, n°25
DOI: 10.1007/s11306-024-02094-2
Status : Postprint (Author's version)

Figure 3.

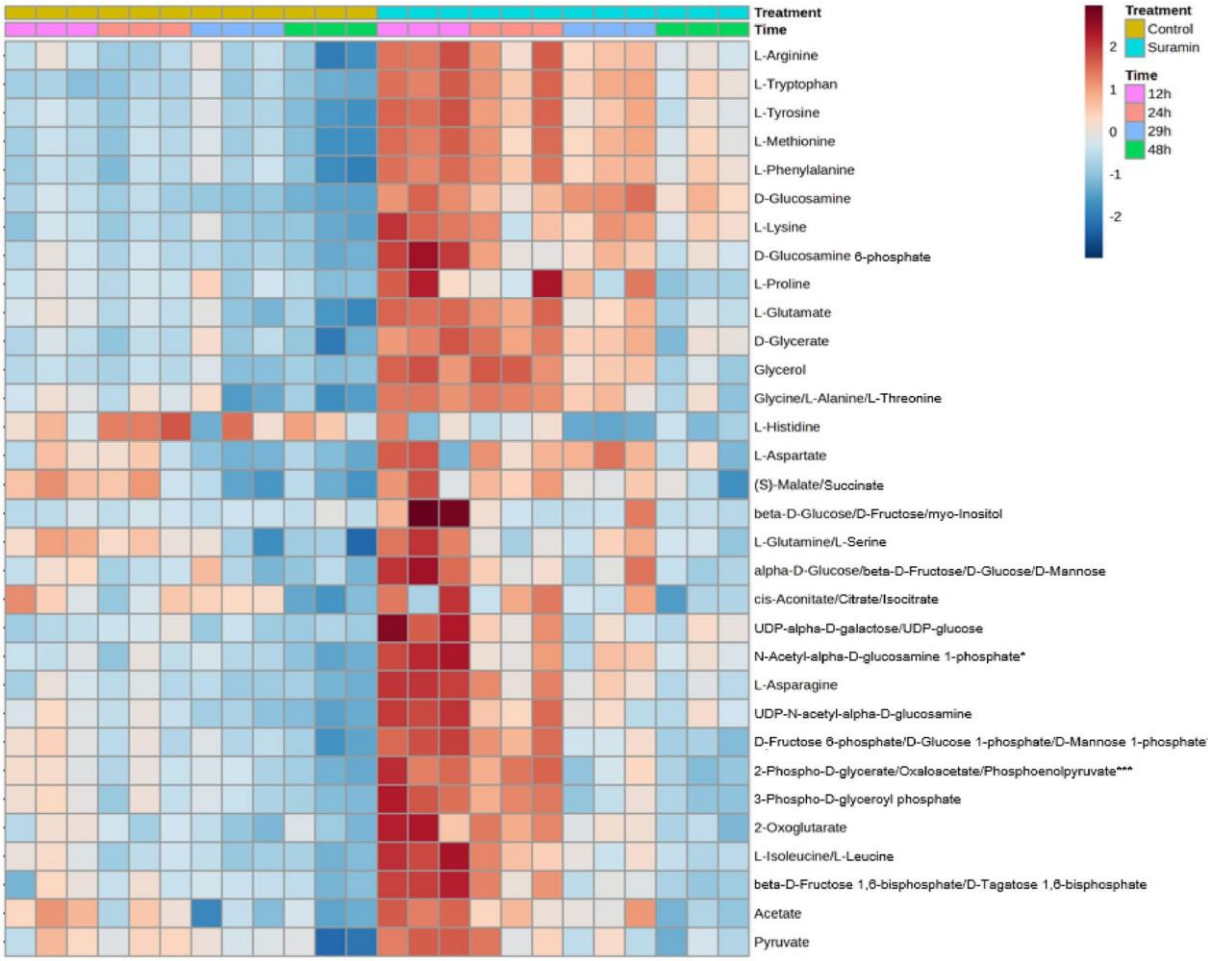

LC-MS-heatmap of significantly altered metabolites reveals diverse effects (treatment, time, and interaction) between control and suramin-treated *T. brucei* groups at different time points in metabolomics analysis" (red color = higher abundance; blue color = lower abundance). Analysis conducted using euclidean distance method with Ward clustering algorithm after normalization to samples median and Pareto scaling.

Published in : Metabolomics (2024), vol. 20, n°25
DOI: 10.1007/s11306-024-02094-2
Status : Postprint (Author's version)

Figure 4.

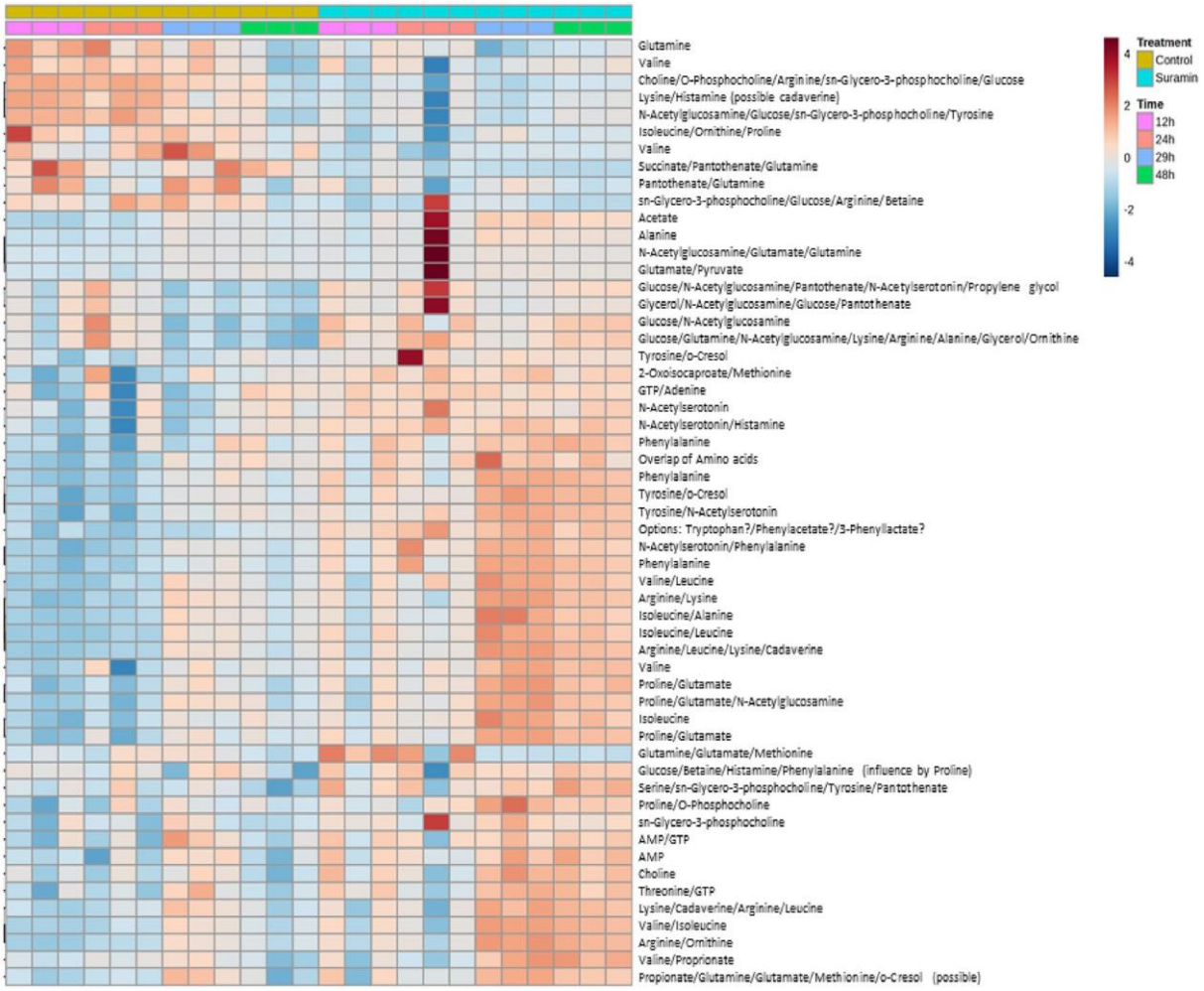

NMR-heatmap of significantly altered metabolites reveals diverse effects (treatment, time, and interaction) between control and suramin-treated *T. brucei* groups at different time points in metabolomics analysis" (red color = higher abundance; blue color = lower abundance). Analysis conducted using euclidean distance method with Ward clustering algorithm after normalization to samples median and Pareto scaling.

Published in : Metabolomics (2024), vol. 20, n°25
DOI: 10.1007/s11306-024-02094-2
Status : Postprint (Author's version)

Figure 5.

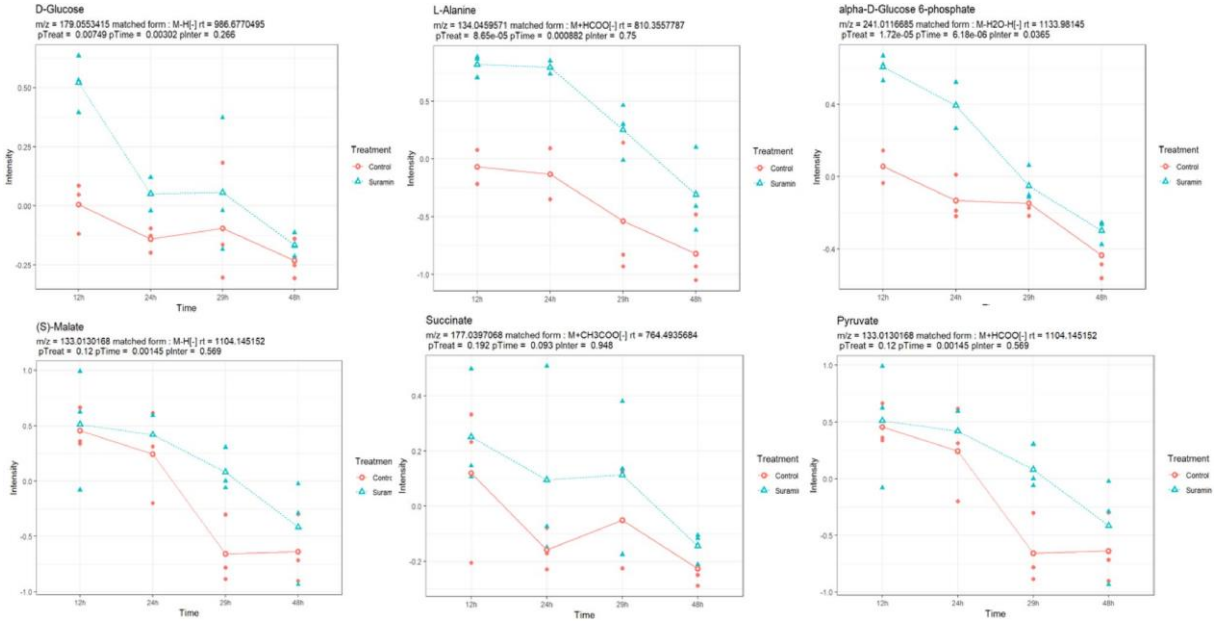

The plot of evolution in time of the mean normalized intensities in MS-negative mode for significant features corresponding to potential compounds in significant pathways.

Published in : Metabolomics (2024), vol. 20, n°25
DOI: 10.1007/s11306-024-02094-2
Status : Postprint (Author's version)

Figure 6.

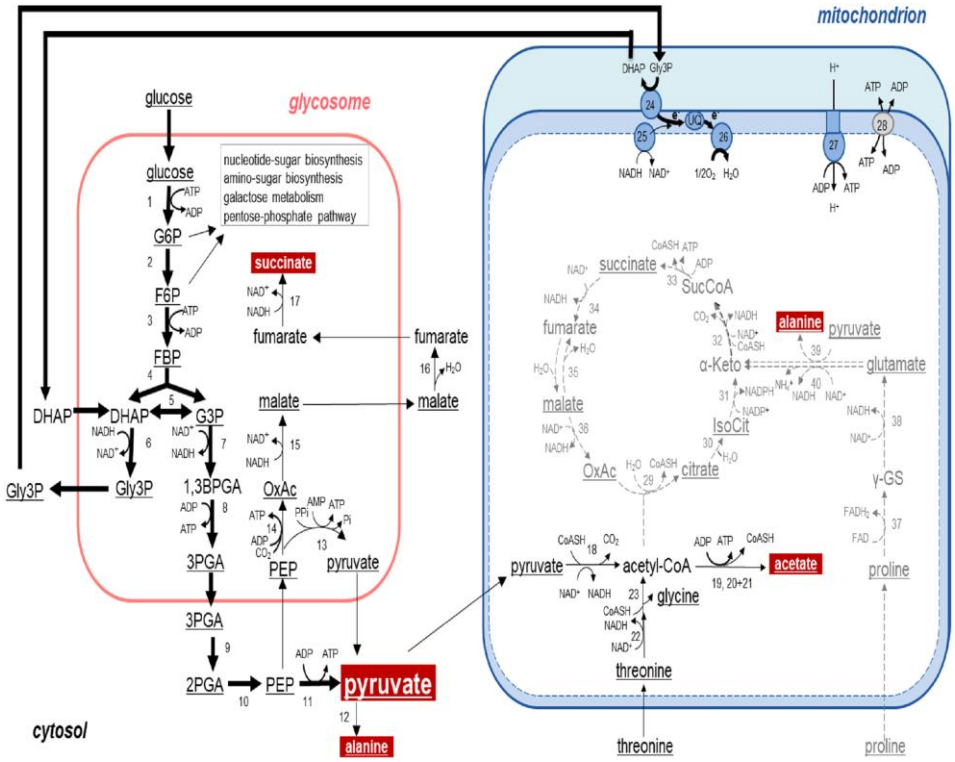

Simplified representation of the intermediary metabolism of BSF *T. brucei*. The trypanosomes use glucose as major free energy source. Glucose, taken up from the environment, is catabolized via glycolysis to pyruvate of which the major part is excreted. A minor fraction of the pyruvate is further metabolized, resulting in the additional end-products alanine, acetate, and succinate. The end-products are shown in white font in boxes against a red background with the size of the boxes reflecting the importance of the flux. Threonine, also taken up by the trypanosomes, may contribute to the acetate production. The major metabolic fluxes of BSF *T. brucei* are also represented by thick black arrows, minor fluxes by thin black arrows. Mitochondrial functions such as the TCA cycle and major parts of the amino-acid metabolism are severely repressed in the BSF trypanosomes (Zíková et al., 2017); they are represented in the scheme in simplified form, in grey and by dashed arrows, because, as reported by Zoltner et al. (2020), upregulated expression of several of the enzymes involved is observed in BSF *T. brucei* two days after addition of suramin to the culture. The highlighted metabolites are those found to be statistically significant in our analyses. Enzymes: 1, hexokinase; 2, glucose-6-phosphate isomerase; 3, phosphofructokinase; 4, aldolase; 5, triose-phosphate isomerase; 6, glycerol-3-phosphate dehydrogenase; 7, glyceraldehyde-3-phosphate dehydrogenase; 8, phosphoglycerate kinase C; 9, phosphoglycerate mutase; 10, enolase; 11, pyruvate kinase; 12, alanine aminotransferase; 13, pyruvate phosphate dikinase; 14, phosphoenolpyruvate carboxykinase; 15, glycosomal malate dehydrogenase; 16, cytosolic fumarase; 17, glyco-somal NADH-dependent fumarate reductase; 18, pyruvate dehydrogenase complex; 19, acetyl-CoA thioesterase; 20, acetate:succinate CoA-transferase; 21, succinyl-CoA synthetase; 22, L-threonine dehydrogenase; 23, 2-amino-3-ketobutyrate CoA-transferase; 24, mitochondrial FAD-dependent glycerol-3-phosphate dehydrogenase; 25, 21, NADH dehydrogenase (complex I of the respiratory chain); 26, alternative oxidase; 27, F_oF1-ATP synthase; 28, ADP/ATP exchange carrier; 29, citrate synthase; 30, aconitase; 31, isocitrate dehydrogenase; 32, a-ketoglutarate dehydrogenase; 33, succinyl-CoA synthetase; 34, mitochondrial NADH-dependent fumarate reductase; 35, mitochondrial fumarase; 36, mitochondrial malate dehydrogenase; 37, L-proline dehydrogenase; 38, pyrroline-5-carboxylate dehydrogenase; 39, alanine aminotransferase; 40, glutamate dehydrogenase. Abbreviations: G6P, glucose 6-phosphate; F6P, fructose 6-phosphate; FBP, fructose 1,6-bisphosphate; DHAP, dihydroxyacetone phosphate; Gly3P, glycerol 3-phosphate; G3P, glyceraldehyde 3-phosphate; 1,3BPGA, 1,3-bisphosphoglycerate; 3PGA, 3-phosphoglycerate; 2PGA, 2-phosphoglycerate; PEP, phosphoenolpyruvate; OxAc, oxaloacetate; PPi, inorganic pyrophosphate; CoASH, coenzyme A; IsoCit, isocitrate; a-Keto, a-ketoglutarate; SucCoA, succinyl-CoA; γ-GS, glutamate γ-semialdehyde; UQ, ubiquinone. The light blue coloured area of the mitochondrion represents the intermembrane space between the mitochondrial outer membrane (not drawn) and the inner membrane (darker blue) containing the respiratory chain complexes, the F_oF_t-ATP synthase and the ADP/ATP exchanger. Figure modified from Michels et al., 2021, where also more details can be found.

Published in : Metabolomics (2024), vol. 20, n°25
DOI: 10.1007/s11306-024-02094-2
Status : Postprint (Author's version)

Table 1. *ASCA data modeling: exploring variance contribution and significance of model effects*

Model effect	Percentage % of variance (Type III)	Bootstrap p-values
MS—negative ionisation		
Treatment	15.7	< 0.002
Time	33.7	< 0.002
Treatment*Time	12.2	0.028
Residual	38.4	—
MS—positive ionisation		
Treatment	8.1	0.010
Time	28.3	< 0.002
Treatment*Time	12.3	0.114
Residual	51.4	—
NMR		
Treatment	32.6	< 0.002
Time	22.4	< 0.002
Treatment*Time	18.2	< 0.002
Residual	24.5	—

Table 2. *Number and percentage of significant metabolites in group differentiation for each ANOVA 2 model effect before and after BH-FDR multiplicity correction.*

Model effect	Number of significant tests	Percentage %	Number of significant tests after FDR correction	Percentage after FDR correction %
MS—negative ionization				
Treatment	717	44	610	37
Time	1061	64	958	58
Interaction	439	27	132	8
MS—negative ionization				
Treatment	429	28	216	14
Time	675	44	513	33
Interaction	188	12	5	0
NMR				
Treatment	96	53	81	45
Time	69	38	48	27
Interaction	16	9	3	2

Published in : Metabolomics (2024), vol. 20, n°25
DOI: 10.1007/s11306-024-02094-2
Status : Postprint (Author's version)

Table 3. *Significant features from LC-MS data in positive mode, potential matches and adjusted p -value per effect.*

m/z	Retention Time (seconds)	Potential match name (Form)	Adjusted treatment p-value	Adjusted time p-value	Adjusted interaction p-value
445.3	234	Menaquinone	0.1547	0.01108	0.2057
303.2	241	(15S)-15-Hydroxy-5,8,11-cis-13-trans-eicosatetraenoate; 5(S)HETE	0.7355	0.0225	0.4323
173	940	D-Ribose; (R)-3-Hydroxybutanoate; (S)-3-Hydroxyisobutyrate	0.0009767	0.004576	0.3272
347	1002	UMP	0.000458	0.002669	0.3271
203.1	1009	D-Glucose D-Fructose; myo-Inositol; D-Mannose; beta-D-Glucose; alpha-D-Glucose; beta-D-Fructose	0.0008335	0.00602	0.3933
400	1026	ADP; GDP; dGDP	0.01738	0.008786	0.7711
125	1027	Phosphoenolpyruvate; Glycerone phosphate; D-Glyceraldehyde 3-phosphate	0.1009	0.0141	0.7012
184.1	1027	Choline phosphate	0.05436	0.01853	0.7012
203.1	1057	D-Glucose; D-Fructose; myo-Inositol; D-Mannose; beta-D-Glucose; alpha-D-Glucose; beta-D-Fructose	0.0002223	0.001128	0.04513
253	1069	D-Ribose 5-phosphate; D-Ribulose 5-phosphate; D-Xylulose 5-phosphate; L-Selenocystathionine	0.01925	0.2649	0.653
437	1069	dTTP	0.0001734	0.0159	0.68
140.9	1077	Fe2 + ; Fe3 +	0.2487	0.04678	0.4145
141	1091	D-Glucono-1,5-lactone 6-phosphate	0.9871	0.04323	0.8419
204.1	1096	Spermidine	0.05189	0.0002378	0.1967
146.1	1097	4-Trimethylammoniobutanoate	0.6752	0.01752	0.7002
135	1099	3-(4-Hydroxyphenyl)pyruvate	0.5663	0.04422	0.7318
161.1	1100	L-Tryptophan	0.4173	0.003613	0.6911
101.1	1102	L-Glutamine	0.6608	0.04313	0.9342
98.98	1105	Acetate	0.4955	0.03928	0.739
506	1178	dCTP	0.008012	0.08416	0.6114
370.1	1217	AMP; dGMP	0.0002223	0.0146	0.4642
368	1292	Orotidine 5'-phosphate	0.002076	0.04823	0.3933
798.8	1599	1-Diphosinositol pentakisphosphate; 5-PP-InsP5	0.4645	0.0259	0.6911
88.04	1843	L-Aspartate; L-Serine; 2-Oxosuccinamate	0.2513	0.02338	0.6872
102.1	1857	L-Threonine; L-Homoserine 2-Oxoglutaramate	0.05353	0.00602	0.1967
176.1	1874	L-Citrulline	0.9323	0.01269	0.08558
122	1889	L-Cysteine	0.06753	0.002509	0.1422
102.1	1909	L-Threonine; L-Homoserine; 2-Oxoglutaramate	0.02719	0.1293	0.3885
262.1	2068	Dihydrobiopterin	0.9939	0.04607	0.4992
421	2093	dTDP	0.2513	0.03036	0.4173
264.1	2095	dAMP	0.8736	0.005705	0.5096
481	2096	dIDP (M + HCOONa	0.199	0.01813	0.3268
298.3	238.2	Sphinganine 1-phosphate	0.02719	0.01249	0.6911
284.3	240.3	Sphinganine	0.02737	0.00889	0.6971
210.2	298.4	5-Dehydroepisterol	0.7891	0.007869	0.8144
195.1	361.3	beta-Alanyl-N(pi)-methyl-L-histidine	0.1561	0.01259	0.7353
140	399.4	Acetyl phosphate	0.9759	0.03624	0.6971
181	400.6	Nicotinamide	0.5899	0.00338	0.5785
223	400.7	D-Erythrose 4-phosphate	0.7444	0.01539	0.5799
117.1	404.1	Dolichyl phosphate D-mannose	0.5737	0.01394	0.3268
89.06	415.9	3-Methyl-2-oxobutanoic acid; Glutarate; 5-Oxopentanoate	0.2741	0.005983	0.8523
202.1	530.3	D-Glucosamine	0.03671	0.2058	0.5997
305.1	580.6	N-((R)-Pantothenoyl)-L-cysteine	0.002208	0.04554	0.8144

Published in : Metabolomics (2024), vol. 20, n°25
DOI: 10.1007/s11306-024-02094-2
Status : Postprint (Author's version)

127	606.1	Imidazole-4-acetate	0.3998	0.006331	0.1422
184.1	819.8	Choline phosphate	0.9877	0.003172	0.6971
113	822.5	Orotate; (S)-Dihydroorotate	0.00403	0.001086	0.9835
153	927.4	(S)-Malate	0.0238	0.03928	0.6976
154	927.9	L-Proline	0.1113	0.01081	0.4971
175	928.1	Citrate; D-Glycerate; Isocitrate; cis-Aconitate	0.01014	0.04348	0.6064
267.1	959.9	Uridine	0.01307	0.01399	0.5932
514.7	963.9	Palmitoyl-CoA	0.1558	0.03877	0.3788
347	987.6	UMP	0.0002419	0.005142	0.4992

Published in : Metabolomics (2024), vol. 20, n°25
DOI: 10.1007/s11306-024-02094-2
Status : Postprint (Author's version)

Table 4. *Significant pathways from the functional analysis of the MS data in negative mode.*

	Pathway	EASE score	Significant potential compounds
Treatment			
	Protein biosynthesis	0.0001278	L-Alanine; L-Glutamate; L-Aspartate; Glycine; L-Threonine; L-Serine; L-Lysine; L-Methionine; L-Proline; L-Histidine; L-Phenylalanine; L-Asparagine; L-Leucine; L-Isoleucine; L-Arginine; L-Tyrosine; L-Tryptophan
	Amino-sugar and nucleotide-sugar metabolism	0.024498	D-Mannose; D-Glucose; alpha-D-Glucose; beta-D-Fructose; D-Glucosamine; alpha-D-Glucose 6-phosphate; beta-D-Fructose 6-phosphate; D-Mannose 1-phosphate; D-Mannose 6-phosphate; D-Glucose 1-phosphate; D-Glucosamine 6-phosphate; N-Acetyl-alpha-D-glucosamine 1-phosphate; N-Acetyl-D-glucosamine 6-phosphate; UDP-alpha-D-galactose; UDP-glucose; UDP-N-acetyl-alpha-D-glucosamine
Time			
	Dicarboxylic acid metabolism / TCA cycle / Amino acid metabolism linked to the TCA cycle (glutamine/glutamate) and linked to glycolysis/ via 3-phosphoglycerate (serine and glycine)	0.018122	Acetate; Pyruvate; L-Glutamate; Succinate; (S)-Malate; Glycine; L-Serine; 2-Oxoglutarate; L-Glutamine; D-Glycerate; 2-Phospho-D-glycerate; Oxaloacetate; 3-Phospho-D-glycerate; cis-Aconitate; Citrate; Isocitrate
Interaction			
	Glycolysis	0.013944	beta-D-Glucose; D-Glucose; alpha-D-Glucose; Phosphoenolpyruvate; 2-Phospho-D-glycerate; Oxaloacetate; 3-Phospho-D-glycerate; alpha-D-Glucose 6-phosphate; beta-D-Fructose 6-phosphate; beta-D-Glucose 6-phosphate; D-Glucose 1-phosphate; 3-Phospho-D-glyceroyl phosphate; beta-D-Fructose 1,6-bisphosphate
	Galactose metabolism	0.03113	Glycerol; D-Mannose; D-Fructose; D-Glucose; alpha-D-Glucose; myo-Inositol; alpha-D-Glucose 6-phosphate; D-Fructose 6-phosphate; D-Tagatose 6-phosphate; D-Glucose 1-phosphate; D-Tagatose 1,6-bisphosphate; UDP-alpha-D-galactose; UDP-glucose

Published in : Metabolomics (2024), vol. 20, n°25
DOI: 10.1007/s11306-024-02094-2
Status : Postprint (Author's version)

Table 5. *Significant metabolite responses to treatment, time, and interaction effects: A comprehensive analysis using LC-MS and NMR.*

Treatment			Time			Interaction		
Metabolite	LC-MS	NMR	Metabolite	LC-MS	NMR	Metabolite	LC-MS	NMR
Alanine	***	***	Acetate	***	**	D-Glucose	**	*
Threonine	***	***	Pyruvate	**	**	Phosphoenolpyruvate/ oxaloacetate/phospho-D-glycerate	*	NS
Glutamate	***	***	L-Glutamate	***	**	Glucose-6-phosphate/glucose-1-phosphate/fructose-6-phosphate	*	NS
Methionine	***	**	Succinate	**	NS	3-Phospho-D-glycerolphosphate	*	NS
Aspartate	**	NS	Malate	**	NS	Beta-D-fructose 1,6 biphosphate	*	NS
Serine	***	***	Glycine	***	NS	Glycerol	*	NS
Lysine	***	***	Serine	**	NS	Glutamine/glutamate/ methionine	NS	**
Proline	*	**	Oxoglutarate	***	NS			
Histidine	**	NS	L-Glutamine	***	*			
Phenylalanine	***	***	D-Glycerate	***	NS			
Asparagine	***	NS	Phospho-D-glycerate	***	NS			
Leucine	***	***	Cis-aconitate	**	NS			
Arginine	***	***	Citrate	*	NS			
Isoleucine	***	***	Isocitrate	*	NS			
Tyrosine	***	***	Valine	NS	***			
Tryptophan	***	NS	Leucine	***	***			
Glucose	**	***	Isoleucine	***	***			

Published in : Metabolomics (2024), vol. 20, n°25
DOI: 10.1007/s11306-024-02094-2
Status : Postprint (Author's version)

D-glucosamine	***	NS	Lysine	*	*
N-acetylglucosamine	NS	***	Alanine	***	***
Alpha-Glucose-6-phosphate	***	NS	Proline	NS	**
Glucosamine-6-phosphate	***	NS	Arginine	***	***
UDP-glucose ou UDP-N-acetylglucosamine	***	NS	Glucose/N-Acetylglucosamine	***	*
AMP	NS	**	Threonine/GTP	***	*
Choline	NS	***	Tyrosine	***	***
sn-Glycero-3-phosphocholine	NS	*	Phenylalanine	**	**
GTP	NS	*			
Histamine	NS	***			
Adenine	NS	*			

'*'—indicates significant metabolite presence according to the analytical method (*p < 0,05; **p < 0,01; ***p < 0,001). 'NS' denotes non-significance or absence of metabolite detection (NMR or LC-MS). A metabolite may be present but non-significant, in which case it is denoted as 'NS'

Published in : Metabolomics (2024), vol. 20, n°25
DOI: 10.1007/s11306-024-02094-2
Status : Postprint (Author's version)

SUPPLEMENTARY INFORMATION The online version contains supplementary material available at https://doi.org/10.1007/s11306-024-02094-2.

AUTHOR CONTRIBUTIONS Conceptualization: Fanta Fall, Joëlle Quetin- Leclercq, Bernadette Govaerts Literature search : Fanta Fall, Madeline Vast, Paul Michels Writing - original draft preparation: Fanta Fall, Paul Michels, Madeline Vast, Lucia Mamede Writing - review and editing: Fanta Fall, Paul Michels, Joëlle Quetin-Leclercq, Lucia Mamede, Bernadette Govaerts, Pascal De Tullio, Michel Frédérich, Marie-Pierre Hayette Supervision: Joëlle Quetin-Leclercq, Bernadette Govaerts

FUNDING This work was funded by Fonds De La Recherche Scientifique - FNRS (grant no. T.0092.20).

DECLARATIONS

CONFLICT OF INTEREST Authors declare no conflict of interest.

Published in : Metabolomics (2024), vol. 20, n°25
DOI: 10.1007/s11306-024-02094-2
Status : Postprint (Author's version)

References

Adusumilli, R., & Mallick, P. (2017). Data conversion with ProteoWizard msConvert. *Methods in Molecular Biology (Clifton, N.J.), 1550*, 339-368. https://doi.org/10.1007/978-1-4939-6747-6_23

Alsford, S., Eckert, S., Baker, N., Glover, L., Sanchez-Flores, A., Leung, K. F., Turner, D. J., Field, M. C., Berriman, M., & Horn, D. (2012). High-throughput decoding of antitrypanosomal drug efficacy and resistance. *Nature, 482*(7384), 232-236. https://doi. org/10.1038/nature10771

Bakker, B. M., Michels, P. A. M., Opperdoes, F. R., & Westerhoff, H. V. (1999). What controls glycolysis in bloodstream form *Trypanosoma brucei* ? *Journal of Biological Chemistry, 274*(21), 1455114559. https://doi.org/10.1074/jbc.274.21.14551

Benjamini, Y., & Hochberg, Y. (1995). Controlling the false discovery rate: A practical and powerful approach to multiple testing. *Journal of the Royal Statistical Society: Series B (Methodological), 57*(1), 289-300. https://doi.org/10.1111/j.2517-6161.1995. tb02031.x

Borchardt, R. T. (2012). Mechanism of drug action: Basic concepts. In *Retrometabolic drug design and targeting* (8th ed., Vol. 74, pp. 9-38). Wiley.

Bringaud, F., Baltz, D., & Baltz, T. (1998). Functional and molecular characterization of a glycosomal PPi-dependent enzyme in trypanosomatids: Pyruvate, phosphate dikinase. *Proceedings of the National Academy of Sciences of the United States of America, 95*(14), 7963-7968. https://doi.org/10.1073/pnas.95.14.7963

Creek, D. J., Mazet, M., Achcar, F., Anderson, J., Kim, D.-H., Kamour, R., Morand, P., Millerioux, Y., Biran, M., Kerkhoven, E. J., Chokkathukalam, A., Weidt, S. K., Burgess, K. E. V., Breitling, R., Watson, D. G., Bringaud, F., & Barrett, M. P. (2015). Probing the metabolic network in bloodstream-form *Trypanosoma brucei* using untargeted metabolomics with stable isotope labelled glucose. *PLoS Pathogens*. https://doi.org/10.1371/journal.ppat. 1004689

Fall, F., Mamede, L., Schioppa, L., Ledoux, A., De Tullio, P., Michels, P., Frédérich, M., & Quetin-Leclercq, J. (2022). Trypanosoma brucei: Metabolomics for analysis of cellular metabolism and drug discovery. *Metabolomics, 18* (4), 20. https://doi.org/10.1007/ s11306-022-01880-0

Giacomoni, F., Le Corguillé, G., Monsoor, M., Landi, M., Pericard, P., Pétéra, M., Duperier, C., Tremblay-Franco, M., Martin, J.-F., Jacob, D., Goulitquer, S., Thévenot, E. A., & Caron, C. (2015). Workflow4Metabolomics: A collaborative research infrastructure

for computational metabolomics. *Bioinformatics, 31* (9), 14931495. https://doi.org/10.1093/bioinformatics/btu813

Hannaert, V. (2011). Sleeping sickness pathogen (Trypanosoma brucei) and natural products: Therapeutic targets and screening systems. *Planta Medica, 77*(6), 586-597. https://doi.org/10.1055/s-0030-1250411

Hirumi, H., & Hirumi, K. (1994). Axenic culture of African trypanosome bloodstream forms. *Parasitology Today, 10*(2), 80-84. https://doi.org/10.1016/0169-4758(94)90402-2

Jansen, J. J., Hoefsloot, H. C. J., Van der Greef, J., Timmerman, M. E., & Smilde, A. K. (2005). ASCA: Analysis of multivariate data obtained from an experimental design. *Journal of Chemometrics, 19*(9), 469-481. https://doi.org/10.1002/cem.952

Published in : Metabolomics (2024), vol. 20, n°25
DOI: 10.1007/s11306-024-02094-2
Status : Postprint (Author's version)

Kazakova, R. R., & Masson, P. (n.d.). Quantitative Measurements of Pharmacological and Toxicological Activity of Molecules. *Chemestry*, *4*(4), 1466-1474. https://doi.org/10.3390/chemistry4 040097

Kushwaha, V., & Capalash, N. (2022). Aminoacyl-tRNA synthetase (AARS) as an attractive drug target in neglected tropical trypanosomatid diseases-Leishmaniasis, Human African Trypanosomiasis and Chagas disease. *Molecular and Biochemical Parasitology, 251*, 111510. https://doi.org/10.1016/j.molbiopara.2022.111510

Li, S., Park, Y., Duraisingham, S., Strobel, F. H., Khan, N., Soltow, Q. A., Jones, D. P., & Pulendran, B. (2013). Predicting network activity from high throughput metabolomics. *PLoS Computational Biology, 9*(7), e1003123. https://doi.org/10.1371/journal. pcbi.1003123

Marchese, L., de Nascimento, J. F., Damasceno, F. S., Bringaud, F., Michels, P. A. M., & Silber, A. M. (2018). The Uptake and metabolism of amino acids, and their unique role in the biology of pathogenic trypanosomatids. *Pathogens, 7*(2), 36. https://doi. org/10.3390/pathogens7020036

Mazet, M., Morand, P., Biran, M., Bouyssou, G., Courtois, P., Daulouède, S., Millerioux, Y., Franconi, J.-M., Vincendeau, P., Moreau, P., & Bringaud, F. (2013). Revisiting the central metabolism of the bloodstream forms of Trypanosoma brucei: Production of acetate in the mitochondrion is essential for parasite viability. *PLoS Neglected Tropical Diseases, 7*(12), e2587. https://doi.org/ 10.1371/journal.pntd.0002587

Michels, P. A. M., & Gualdrón-López, M. (2022). Biogenesis and metabolic homeostasis of trypanosomatid glycosomes: New insights and new questions. *The Journal of Eukaryotic Microbiology, 69* (6), e12897. https://doi.org/10.1111/jeu.12897

Michels, P. A. M., Villafraz, O., Pineda, E., Alencar, M. B., Cáceres, A. J., Silber, A. M., & Bringaud, F. (2021). Carbohydrate metabolism in trypanosomatids: New insights revealing novel complexity, diversity and species-unique features. *Experimental Parasitology, 224*, 108102. https://doi.org/10.1016Zj.exppai-a.2021.108102

Misset, O., Bos, O. J., & Opperdoes, F. R. (1986). Glycolytic enzymes of *Trypanosoma brucei*. Simultaneous purification, intraglycosomal concentrations and physical properties. *European Journal of Biochemistry, 157*(2), 441-453. https://doi.org/10.1111/j.1432-1033.1986.tb09687.x

Morgan, H. P., Zhong, W., McNae, I. W., Michels, P. A. M., Fothergill-Gilmore, L. A., & Walkinshaw, M. D. (2014). Structures of pyruvate kinases display evolutionarily divergent allosteric strategies. *Royal Society Open Science, 1* (1), 140120. https://doi.org/ 10.1098/rsos.140120

Nare, Z., Moses, T., Burgess, K., Schnaufer, A., Walkinshaw, M. D., & Michels, P. A. M. (2023). Metabolic insights into phosphofructokinase inhibition in bloodstream-form trypanosomes. *Frontiers in Cellular and Infection Microbiology, 13*, 1129791. https://doi. org/10.3389/fcimb.2023.1129791

Nascimento, J. F., Souza, R. O. O., Alencar, M. B., Marsiccobetre, S., Murillo, A. M., Damasceno, F. S., Girard, R. B. M. M., Marchese, L., Luevano-Martinez, L. A., Achjian, R. W.,

Haanstra, J. R., Michels, P. A. M., & Silber, A. M. (2023). How much (ATP) does it cost to build a trypanosome? A theoretical study on the quantity of ATP needed to maintain and duplicate a bloodstream-form Trypanosoma brucei cell. *PLoS Pathogens, 19* (7), e1011522. https://doi.org/10.1371/journal.ppat.1011522

Nasim, F., & Qureshi, I. A. (2023). Aminoacyl tRNA synthetases: Implications of structural biology in drug development against trypanosomatid parasites. *ACS Omega, 8*(17), 14884-14899. https://doi.org/10.1021/acsomega.3c00826

Published in : Metabolomics (2024), vol. 20, n°25
DOI: 10.1007/s11306-024-02094-2
Status : Postprint (Author's version)

NMR-based Metabolomics. (2018). The Royal Society of Chemistry. https://doi.org/10.1039/9781782627937

Opperdoes, F. R., & Borst, P. (1977). Localization of nine glycolytic enzymes in a microbody-like organelle in Trypanosoma brucei: The glycosome. *FEBS Letters, 80*(2), 360-364. https://doi.org/ 10.1016/0014-5793(77)80476-6

Pang, Z., Chong, J., Li, S., & Xia, J. (2020). MetaboAnalystR 3.0: Toward an optimized workflow for global metabolomics. *Metabolites, 10* (5), 186. https://doi.org/10.3390/metabo10050186

Pang, Z., Chong, J., Zhou, G., de Lima Morais, D. A., Chang, L., Barrette, M., Gauthier, C., Jacques, P. -E., Li, S., & Xia, J. (2021). MetaboAnalyst 5.0: Narrowing the gap between raw spectra and functional insights. *Nucleic Acids Research, 49*(1), W388-W396. https://doi.org/10.1093/nar/gkab382

Steverding, D., & Troeberg, L. (2023). 100 years since the publication of the suramin formula. *Parasitology Research, 123*(1), 11. https://doi.org/10.1007/s00436-023-08027-7

Thiel, M., Benaiche, N., Martin, M., Franceschini, S., Van Oirbeek, R., & Govaerts, B. (2023). limpca: An R package for the linear modeling of high-dimensional designed data based on ASCA/ APCA family of methods. *Journal of Chemometrics, 37*(7), e3482. https://doi.org/10.1002/cem.3482

Thiel, M., Feraud, B., & Govaerts, B. (2017). ASCA+ and APCA+: Extensions of ASCA and APCA in the analysis of unbalanced multifactorial designs: Analyzing unbalanced multifactorial designs with ASCA+ and APCA+. *Journal of Chemometrics, 31* (6), e2895. https://doi.org/10.1002/cem.2895

Vincent, I. M., & Barrett, M. P. (2015). Metabolomic-based strategies for anti-parasite drug discovery. *Journal of Biomolecular Screening, 20*(1), 44-55. https://doi.org/10.1177/1087057114 551519

Wiedemar, N., Hauser, D. A., & Mäser, P. (2020). 100 Years of Suramin. *Antimicrobial Agents and Chemotherapy*. https://doi. org/10.1128/AAC.01168-19

Wiemer, E. A., Michels, P. A., & Opperdoes, F. R. (1995). The inhibition of pyruvate transport across the plasma membrane of the bloodstream form of Trypanosoma brucei and its metabolic implications. *The Biochemical Journal, 312*(Pt 2), 479-484. https://doi. org/10.1042/bj3120479

Willson, M., Callens, M., Kuntz, D. A., Perie, J., & Opperdoes, F. R. (1993). Synthesis and activity of inhibitors highly specific for the glycolytic enzymes from Trypanosoma brucei. *Molecular and Biochemical Parasitology, 59*(2), 201-210. https://doi.org/ 10.1016/0166-6851(93)90218-m

Wishart, D. S., Tzur, D., Knox, C., Eisner, R., Guo, A. C., Young, N., Cheng, D., Jewell, K., Arndt, D., Sawhney, S., Fung, C., Nikolai, L., Lewis, M., Coutouly, M.-A., Forsythe, I., Tang, P., Shrivastava, S., Jeroncic, K., Stothard, P., ... Querengesser, L. (2007). HMDB: The Human Metabolome Database. *Nucleic Acids Research*, *35* (Database issue), D521-526. https://doi.org/10.1093/ nar/gkl923

Wishart, D. S. (2010). Computational approaches to metabolomics. *Methods in Molecular Biology (Clifton, N.J.), 593*, 283-313. https://doi.org/10.1007/978-1-60327-194-3_14

Zíková, A., Verner, Z., Nenarokova, A., Michels, P. A. M., & Lukes, J. (2017). A paradigm shift: The mitoproteomes of procyclic and bloodstream Trypanosoma brucei are comparably complex. *PLoS*

Pathogens, 13 (12), e1006679. https://doi.org/10.1371/journal. ppat.1006679

Zoltner, M., Campagnaro, G. D., Taleva, G., Burrell, A., Cerone, M., Leung, K.-F., Achcar, F., Horn, D., Vaughan, S., Gadelha, C., Zíková, A., Barrett, M. P., de Koning, H. P., & Field, M. C. (2020). Suramin exposure

Published in : Metabolomics (2024), vol. 20, n°25
DOI: 10.1007/s11306-024-02094-2
Status : Postprint (Author's version)

alters cellular metabolism and mitochondrial energy production in African trypanosomes. *Journal of Biological Chemistry*. https://doi.org/10.1074/jbc.RA120.012355

Zoltner, M., Leung, K. F., Alsford, S., Horn, D., & Field, M. C. (2015). Modulation of the surface proteome through multiple ubiquitylation pathways in African trypanosomes. *PLoS Pathogens, 11* (10), e1005236. https://doi.org/10.1371/journal.ppat.1005236